This is the peer reviewed version of the following article:

C. Wäckerlin and K.-H. Ernst, Autocatalytic Surface Explosion Chemistry of 2D Metal-Organic Frameworks, J. Phys. Chem. C, 2021, acs.jpcc.1c03809, which has been published in final form at https://dx.doi.org/10.1021/acs.jpcc.1c03809.

Autocatalytic Surface Explosion Chemistry of 2D Metal-Organic Frameworks

Christian Wäckerlin,[†,*] *and Karl-Heinz Ernst*[†,‡,§,*]

[†] Surface Science and Coating Technologies, Empa - Swiss Federal Laboratories for Materials Research and Technology, Überlandstrasse 129, CH-8600 Dübendorf, Switzerland, E-mail: christian.waeckerlin@empa.ch; karl-heinz.ernst@empa.ch

[‡] Department of Chemistry, University of Zurich, Winterthurerstrasse 190, CH-8057 Zürich, Switzerland

[§] Nanosurf Laboratory, Institute of Physics, The Czech Academy of Sciences, Cukrovarnická 10, 162 00 Prague, Czech Republic

ABSTRACT: Metal-organic frameworks are a combination of inorganic constituents and organic ligands with a high degree of variability which are, as coordination compounds in homogeneous catalysis, potentially highly selective heterogeneous catalysts. The synthesis and thermal stability of monolayer thin Cu-, Ni- and Fe-squarate 2D MOFs is studied using X-ray photoelectron spectroscopy, scanning tunneling microscopy and temperature programmed reaction spectroscopy on a Cu(100) surface in ultrahigh vacuum. Highly ordered 2D squarate MOFs are obtained by mild annealing of squarate multilayers. Upon annealing at higher temperatures, the Ni- and Fe-squarate layers undergo autocatalytic surface explosion chemistry with carbon monoxide as desorbing

product in a very narrow temperature interval. Despite the different stabilities of Ni- and Fe-based MOFs, mixed {Ni+Fe}-MOFs also decompose in a narrow single temperature interval. Such autocatalytic behavior is explained by a numerical model which – unlike rate equation-based kinetics – explicitly considers the chemical nature of nearest neighbors.

TABLE OF CONTENTS ARTWORK

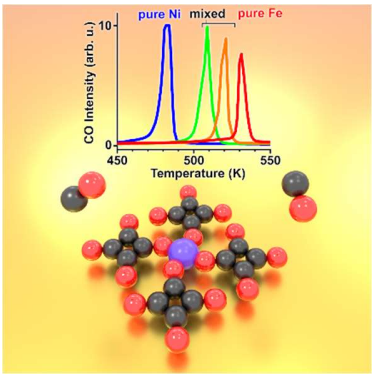

INTRODUCTION

Metal-organic frameworks (MOFs)[1,2] and their two-dimensional (2D) or thin film equivalents are promising candidates as heterogeneous catalysts.[3,4] By the choice of ligands, the charge transfer into the d-states of the central metal atom and consequently the strength of the metal–adsorbate bond can be tuned.[5] Hence, MOF surfaces combine the single atom selectivity of homogeneous catalysis with the sustainability of the solid support of heterogeneous catalysts.[6] Their tunability of selectivity by the choice of organic ligands should be superior to common single atom catalysts, although thermal stability may only allow reactions performed in solution.[7] Moreover, the choice of organic ligand size provides a handle on active site density. In this regard, oxocarbon ligands, composed exclusively of oxygen and carbon atoms, are very interesting as relatively small ligands.[8] Apart from simple molecules like carbon monoxide and dioxide or the linear suboxides, the dianions of cyclic oxocarbons show remarkable stability due to their aromaticity.[8–12] The three

to six-membered cyclooxocarbon dianions (deltate, squarate, croconate and rhodizonate) formed by two-fold deprotonation of their diacids have intriguing properties, such as strong absorption in the UV/vis region, planarity and $D_{\{3\text{-}6\}h}$ symmetry.[13,14]

Autocatalytic reactions are observed in many areas of chemistry, such as radical polymerization, the Butlerov reaction,[15,16] the Soai reaction,[17] and DNA replication, to name a few. Because a reaction product serves as catalyst, the reaction rate is enhanced exponentially after initiation. The autocatalytic decomposition of molecules on surfaces, so-called surface explosion,[18–22] leads commonly to desorption of product in an narrow temperature interval.[18,19,23] Examples are carboxylic acids on metal surfaces,[20,24–27] NO + CO and NO + H_2 on platinum,[28,29] as well as polycyclic hydrocarbons on oxygen covered copper surfaces.[30] In surface explosion the catalyzing product are vacancies in the surface layer.[19] That is, new empty surface sites (*) – which catalyze further decomposition – are created by decomposition of an adsorbed species (A_{ads}) and desorption of product (B↑):[19]

$$A_{ads} + * \rightarrow B\uparrow + 2\,*$$

Therefore, a dense layer without empty sites is stable up to a point at which vacancies are inevitably created that catalyze further decomposition.

Scheme 1. Squaric acid and its dianion squarate.

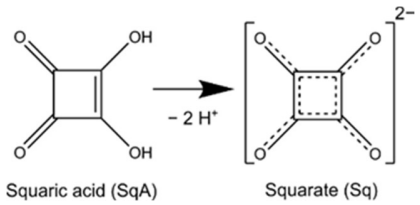

In this letter, the autocatalytic decomposition of a 2D metal-organic frameworks (MOFs) built-up with the dianion squarate (Sq^{2-}) as ligands and Cu^{2+}, Ni^{2+} and Fe^{2+} ions as coordinating metals, synthesized on the 4-fold symmetric Cu(100) surface in ultra-high vacuum is reported. After adsorption of squaric acid (SqA)[31] and its deprotonation into the dianion squarate (Sq^{2-}) (Scheme 1) by complexation of Cu adatoms upon mild annealing, highly ordered 2D metal-organic frameworks (MOFs) are observed by scanning tunneling microscopy (STM). Ni- or/and Fe-MOFs are obtained by co-deposition of Ni or/and Fe atoms to the multilayer prior to annealing. Further annealing leads to decomposition of all MOFs into carbon monoxide, desorbing from the surface, and surface-bound metals. While pure copper MOFs undergo regular decomposition over a wide temperature interval, Ni- and Fe-squarate MOFs decompose autocatalytically in a narrow temperature interval of just a few Kelvin. Although the two components in mixed Fe+Ni squarate MOFs have different stabilities, just a single narrow decomposition signal is observed. Such unique autocatalytic behavior is rationalized here by a kinetic model that takes a synergistic mechanism in form of the nature of nearest neighbors of each squarate unit into account.

EXPERIMENTAL METHODS AND MATERIALS

The experiments are performed in ultrahigh vacuum ($p < 10^{-9}$ mbar). The Cu(100) substrate is cleaned by Ar^+ ion sputtering and annealing cycles. SqA (3,4-dihydroxy-3-cyclobutene-1,2-dione, Sigma Aldrich, purity 99%) and Fe and Ni atoms are sublimed by resistively and electron beam heated sources, respectively. A multilayer (3 – 5 molecular layers) of SqA is deposited onto the sample kept at room temperature, followed by deposition of Ni or Fe. X-ray photoelectron spectroscopy (XPS) data and constant current STM images are recorded at room temperature. Temperature programmed reaction spectroscopy (TPRS) data are obtained using a quadrupole mass spectrometer. A special housing (Feulner cup) with a pinhole is used to avoid collecting

material from the sample holder. Detailed experimental methods are provided in the supporting information (SI).

RESULTS AND DISCUSSION

X-ray Photoelectron Spectroscopy

XPS is used to analyze the chemistry of the transformation into Cu-, Fe- and Ni-squarate layers. Figure 1a,b shows C 1s and O 1s XP spectra of a multilayer (3-5 ML; ML = 1 layer) of SqA on Cu(100) and after mild annealing of all three systems. The O 1s spectra show two components which are identified as C-O*H (533.4 eV) and C=O* (531.4 eV), respectively.[32,33] Annealing of SqA multilayers to 393 K leads to desorption of the multilayers, leaving behind a single layer of molecules. The presence of only one peak O 1s at 531.4 eV (C=O*) and disappearance of the C-O*H peak at 533.4 eV evidences the two-fold dehydrogenation of SqA and the formation of squarate (Sq). As for dehydrogenation of free-base porphyrins and porphyrinoids,[5,34–36] carboxylic acids,[32,37,38] as well as other ligands[39,40] on copper surfaces, Sq forms coordination compounds with Cu adatoms, such that a CuSq layer forms. In all cases, the C/O ratio agrees well with the expected stoichiometry of 1:1 (Table S1).

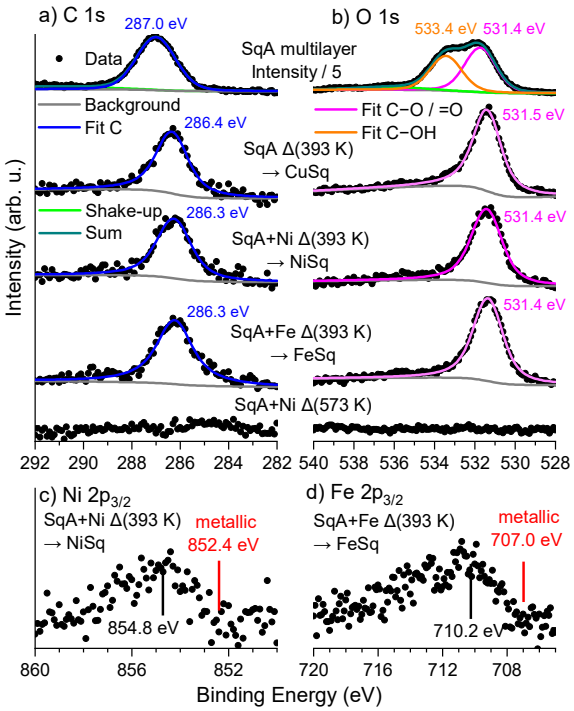

Figure 1. XP spectra showing the transition from SqA multilayers to 2D squarate MOFs on Cu(100). C 1s (a) and O 1s (b) peaks show a pronounced shift to lower binding energies upon annealing to 393 K due to desorption of the Sq multilayer and formation of Cu-, Ni- and Fe-squarate complexes. Annealing to 573 K leads to the disappearance of the O 1s and C 1s signals due to decomposition of the MOFs. XP signals of Ni and Fe core levels (c,d) confirm the ionic character of the respective metal atoms in the MOFs.

Co-deposition of small amounts of Ni or Fe atoms onto the SqA multilayer followed by annealing to 393 K leads to Ni- and FeSq MOFs. The O 1s and C 1s XP signals of Ni- and FeSq are virtually identical to the ones of CuSq, indicating the same chemical SqA → Sq transformation. In contrast to bulk transition metal squarate complexes obtained in solution,[41] here the 2D MOFs do not contain water.

With respect to metallic Ni and Fe clusters on copper,[34] bulk Fe and bulk Ni,[42] binding energy shifts of +2 eV and +3 eV are observed for the Ni $2p_{3/2}$ peak in NiSq (Figure 1c) and the Fe $2p_{3/2}$

peak in FeSq (Figure 1d), respectively. The binding energies are in agreement with ionic Ni(II) and Fe(II) complexes (see detailed discussion in SI).[43] For all three types of MOFs, annealing to 573 K leads to the disappearance of the O 1s and C 1s signals due to decomposition of the MOFs (Figure 1). The metal atoms remain at the surface in metallic form (cf. Figure S1 for Ni $2p_{3/2}$ XP spectra).

Scanning Tunnelling Microscopy

Structure and morphology of the 2D MOFs is best analyzed by STM. Figure 2 shows STM images of Cu-, Ni- and FeSq layers on Cu(100). CuSq forms a square lattice appearing as "flower"-like features (Figure 2a). Two mirror domains are formed (Figure 2b,2c). The two mirror domains reflect the fact that there are two possibilities to arrange the square molecular unit cell on the four-fold symmetric Cu(100) substrate. From comparison with the atomic resolution micrograph of the clean surface (Figure 2d), the registry of the MOF lattice with the Cu(100) surface is $(5\ \mp 1;\ \pm 1\ 5)$ in matrix notation. This (2 × 2) transformation matrix, linking the adsorbate lattice vectors to the substrate lattice vectors, is written here as (upper row; lower row).[44]

As it delivers the stoichiometry and the absolute coverage, XPS is important for deduction of the MOF structures. The O 1s to Cu 2p peak intensity ratio of the CuSq layer is 3.18 times larger than the intensity of the O 1s peak of a O-$(2\sqrt{2}\times\sqrt{2})$R45° structure on Cu(100).[30,45] The latter has ½ an oxygen atom per surface copper atom. Considering the attenuation of the Cu 2p signal to 79% of its previous value (see SI), it can be calculated that the CuSq (5, 1) unit cell contains 8 Sq molecules. Figure 2e shows a structural model with the Cu(100) lattice superimposed: the "flowers" consist of 4 Sq molecules (cyan) coordinating a faintly observable copper atom (Figure 2c). The images also show the weaker contrast of four molecules per unit cell at the corners of the

pink and blue squares (red molecules). The structural model is shown in Figure 2f. For the sake of electric charge neutrality, the unit cell must contain overall 8 Cu atoms.

Interestingly, incorporation of Fe and Ni atoms yields again a (5, 1) structure (Figure 2g,h,j-l). Addition of increasing amounts of Fe leads to the suppression of the "flower" contrast and to the appearance of bright protrusions in their place (Figure 2g,h). The areal density of bright protrusions in STM scales linearly with the coverage of Fe atoms determined by XPS (Figure 2i). This confirms that the bright contrast originates from the Fe atoms and it also shows that virtually all Fe is embedded in the ordered Fe-squarate lattice. The Ni and Fe atoms (Figure 2f, red circles) are accommodated only in the center of the Sq tetramers. As for the pure Cu-MOF, the structural model for the Ni- and Fe-MOFs (Figure 2f) considers 6 additional Cu(II) adatoms. The "ridges" observable next to the bold blue square in Figure 2g as well as in the images of Fe- and NiSq at low bias voltage (Figure 2k,l) may be formed by these Cu adatoms or by a more complex squarate induced surface reconstruction. In any case, this structure renders the bright (cyan molecules) and dark (red molecules) tetrameters non-equivalent (Figure 2e) explaining the different STM contrast of the two types of tetramers. The Ni- and Fe- MOFs must therefore be considered as mixed Ni/Cu and Fe/Cu MOFs.

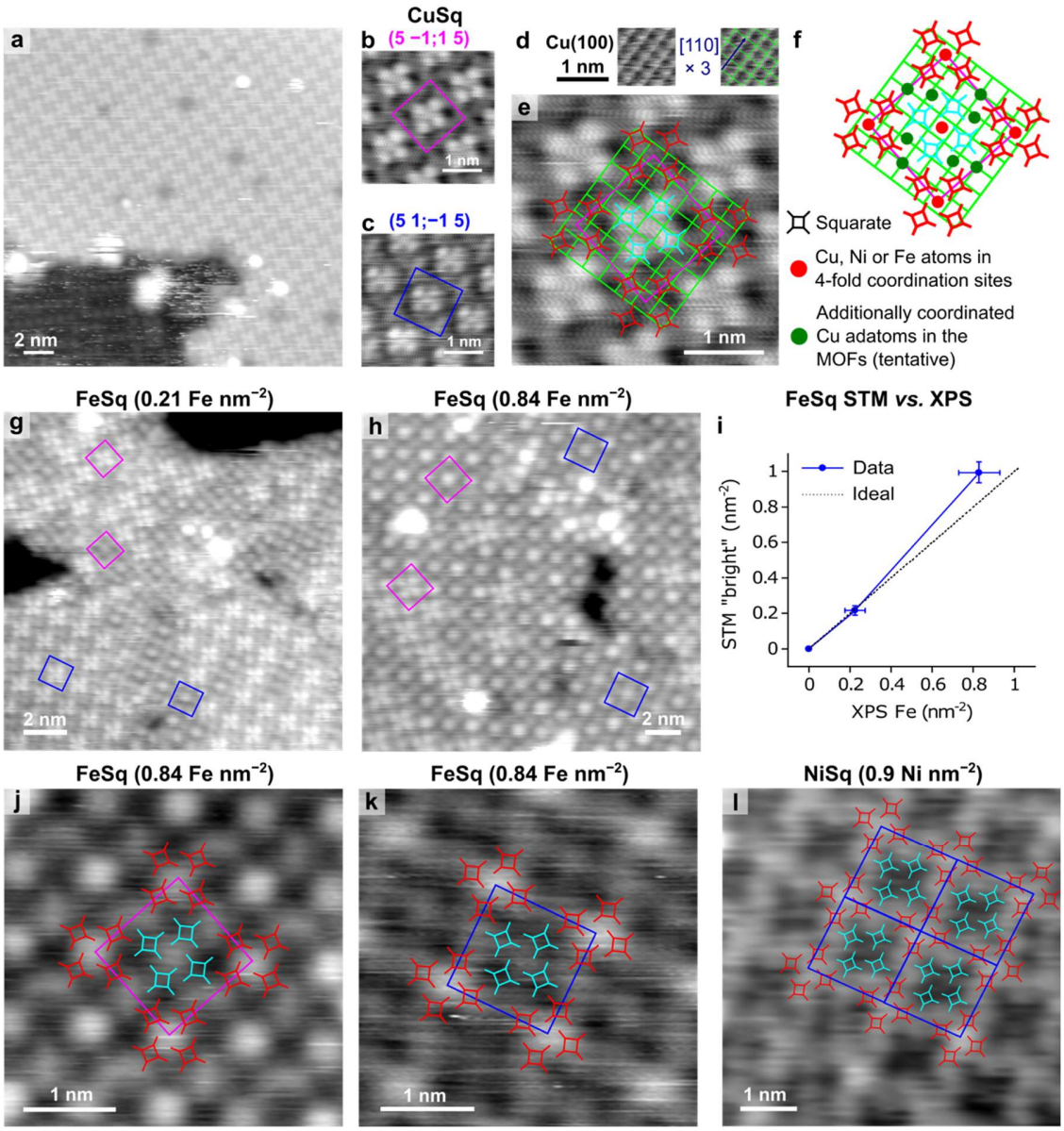

Figure 2. STM images of Cu-, Ni- and FeSq layers on Cu(100). All three layers exist as two mirror domains with the same $(5 \mp 1;\ \pm 1\ 5)$ unit cells. The layers contain 8 molecules per unit cell (structural overlay in f), as determined by XPS (see text). (a-c,e,f) In case of CuSq, the central 4 molecules are imaged with a characteristic "flower" pattern. (g,h) With increasing Fe dose, the "flowers" are progressively replaced with bright protrusions which correspond to the Fe atoms. (i) The areal density of protrusions agrees well with the density of Fe determined by XPS. (j-l) Images

recorded at low bias voltages reveal a different contrast, allowing to image the "ridge-contrast" connecting every second {Fe,Ni} center. Imaging parameters (bias voltage, tunneling current set point): a) 1.85 V, 120 pA; b) 1.85 V, 110 pA; c) 1.85 V, 140 pA; d) 15 mV, ~2 nA constant height image; e) same as b); g) 2.1 V, 130 pA; h) 2.4 V, 150 pA; j) 670 mV, 190 pA; k) 300 mV, 200 pA; l) 30 mV, 70 pA.

Temperature Programmed Reaction Spectroscopy

The decomposition chemistry of Cu-, Ni-, FeSq MOFs is discussed on the basis of the CO (*m/z* = 28 u/e^-) TPR spectra (Figure 3). The Sq ligand decomposes into CO upon heating, while Cu, Ni and Fe remain on the surface. Note that pure CO desorbs from Cu(100) at 190 K under UHV conditions.[46] Hence, upon formation by Sq decomposition CO leaves quasi instantaneously the hot surface and the TPR signal represents the rate-determining step of the MOF decomposition reaction. With increasing squarate coverage and fixed Ni coverage the TPRS peak narrows and shifts to higher temperature (Figure 3a). This shift of the TPRS signal and its narrowing with increasing Sq coverage is the hallmark of autocatalytic surface explosion: a densely packed, saturated layer is stabilized by the absence of vacancies.[47] Saturated Ni-, Fe- and mixed {Fe+Ni}Sq layers decompose each within a single narrow TPR peak (NiSq: 481 K, FeSq: 531 K, mixed layers at intermediate temperatures, see Figure 3c). At full Sq coverage with decreasing amounts of Ni, the resulting mixed {Ni,Cu}Sq layers decompose at progressively higher temperatures in increasingly broad decomposition peaks (Figure 3b). Finally, the saturated pure CuSq layer decomposes over a wide temperature range with maximum at 570 K (Figure 3b). Hence, the autocatalytic decomposition is enabled by vacant sites on the sample allowing the liberation of Ni (or Fe) atoms in the process that, in turn, dramatically increase the rate of decomposition. Such

mechanism leads to the creation of more vacant space and the release of more Ni (or Fe) atoms which speeds up the reaction.

Kinetic Modelling of TPR Spectra

Based on a simple rate equation approach previously used to describe surface explosions,[47] TPR spectra as function of Ni and Sq coverage (Figure S2) and the TPR signals of saturated, pure Ni- and FeSq layers are reproduced (Figure 3d). The model considers regular decomposition (rates are proportional to the coverages θ of CuSq, NiSq, FeSq, respectively) and autocatalytic decomposition for Ni- and FeSq (but not for CuSq), in which the rates are proportional to the coverage of vacancies $\theta_* = 1 - \theta_{CuSq} - \theta_{NiSq} - \theta_{FeSq}$. Rate equations and parameters are found in the SI. However, for mixed {Fe+Ni}Sq layers a rate equation model considering only vacancies as autocatalytic element does not reproduce the narrow TPR signals. Because NiSq decomposes at a lower temperature than FeSq, the number of vacancies starts to increase in the pure rate equation model before the more stable FeSq decomposes. Such early presence of vacancies essentially deactivates the surface explosion of mixed Sq layers in the rate equation model. Instead of a single peak as observed, two peaks evolve in the model (Figure 3d).

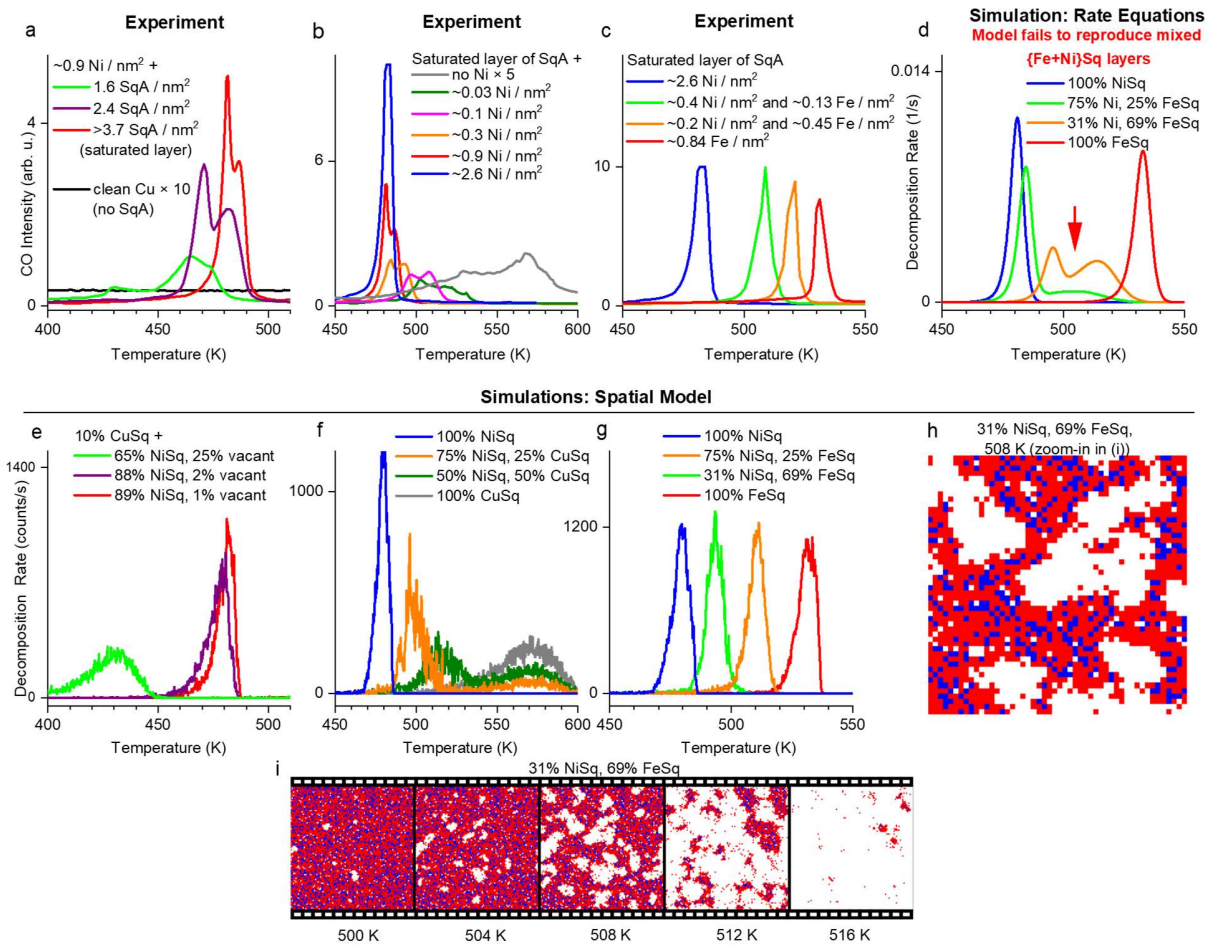

Figure 3. Temperature programmed reaction (TPR) spectra (heating rate 1 K/s) showing the thermally induced decomposition of Cu-, Ni- and FeSq MOFs into carbon monoxide. (a) CO TPR spectra of Sq layers with increasing molecular coverage at fixed Ni coverage. (b) CO TPR spectra of Sq layers with increasing Ni coverage at fixed molecular coverage. (c) CO TPR spectra with different Ni/Fe ratio showing that Ni-, Fe- and mixed {Fe,N}Sq layers decompose autocatalytically in a single narrow TPR peak. (d) Theoretical TPR peaks based on a rate equation model agree with experimental TPR traces of pure Ni- and FeSq layers but disagree in case of mixed {Fe+Ni} systems (red arrow). (e-g) Simulated TPR spectra based on a 2D spatial model, taking the nature of an adjacent site into account, reproduce experimental observation

qualitatively. Because the model is based on decomposition of discrete sites, the simulated spectra exhibit visible noise. (h, i) Modeled 100 × 100 pixels maps showing the course of decomposition with arbitrary positioning of Ni- and FeSq (red: FeSq, blue: NiSq, white: vacancy). As the activation energy for decomposition of FeSq is higher than the one for NiSq, FeSq cells accumulate at the decomposition fronts.

In all previous reports on surface explosion of organic molecules, vacancies were solely defined as the autocatalytic component.[18–26,47,48] However, the concerted decomposition of mixed {Fe+Ni}Sq layers can be best understood if the spatial distribution of Ni-, Fe-, and CuSq cells in connection to the vacancies is considered. By modelling the layer as 2D array of cells, in which every cell has defined neighbors, the experimental TPR traces are reproduced. Depending if the adjacent cells are vacant or occupied, a cell does decompose with different probability. In such "spatial model" with an initial random configuration distribution, the temperature is ramped linearly in discrete time steps. At every time step, the cells can decompose with probability $p = \nu \times \exp(-E_A / (R \times T) \times \Delta t$, where ν is the pre-exponential factor at the standard value of $\nu = 10^{13}$ Hz,[49] R is the gas constant, T the temperature, Δt the length of the time step and E_A is the activation energy of the given species. The TPR spectra are obtained by summation of the decomposition events of all cells. With $E_A^{CuSq} = 156$ kJ/mol for decomposition of CuSq, the basic features of the experimental CuSq TPR spectra (Figure 3b,e) are reproduced and the same TPR trace as obtained from the pure rate equation modelling results (Figure S4). The autocatalytic decomposition of Ni- and FeSq layers is implemented by introducing lower activation energies for decomposition if a cell is located next to vacancies. The model is based on the following assumptions: If 3 or more of the 8 adjacent sites are vacant, the NiSq (or FeSq) cell can decompose with an activation energy of 114 (or 128) kJ/mol. If this is not the case within the timestep, the NiSq (FeSq) cells decompose

with activation energies that are 30 kJ/mol higher, *i.e.* 144 (158) kJ/mol. The activation energies are obtained by fitting the TPRS peak positions. The stabilization energy of 30 kJ/mol determines the width of the TPR peaks of saturated Ni- and FeSq layers. A threshold value of 3 or more adjacent vacancies has been found to best reproduce the behavior of mixed layers. Details of the implementation are provided in the SI.

The facilitated decomposition of Fe- and NiSq cells adjacent to vacancies introduces the autocatalytic dependence on vacancies in the simulations and allows to reproduce all key features of the experimental data, namely: i) early decomposition in case of a low Sq coverage due to a presence of initial vacancies (Figure 3a,e), ii) delayed decomposition of saturated {Ni+Cu}Sq layers obtained at lower Ni coverages due to the higher stability of CuSq (Figure 3b,f), and most important iii) the narrow TPR signals of mixed {Fe+Ni}Sq layers (Figure 3c,g). The layers decompose autocatalytically by formation of vacancy islands and advancing decomposition fronts (Figure 3i and SI movies). In the case of mixed {Fe+Ni} layers, FeSq is accumulated at the decomposition fronts (Figure 3h and SI movies) because FeSq is more stable than NiSq. Hence, less stable NiSq is protected from contact with vacancies and the mixed layers decompose in a single, narrow TPRS peak. Note that, the formation of vacancy islands is reminiscent of the decomposition pattern obtained by the "circular island model".[48] However, the island model is purely analytical and does not consider multiple species.

Although the spatial model can explain the basic characteristics of the autocatalytic decomposition including the cooperative decomposition of mixed {Fe+Ni}Sq layers, it neglects diffusion. However, a MOF is a rigid lattice and the rate of 'explosion' should clearly outnumber diffusion rates of Sq at island edges. Then diffusion of free Ni or Fe may even raise the rate of decomposition due to their catalytic activity. Because diffusion of reactive Ni atoms is not

considered, for Ni-undersaturated {Ni+Cu}Sq layers the model shows peaks at 570 K due to CuSq decomposition (Figure 3f, green and orange spectra) which are absent in the TPRS data (Figure 3b, orange, pink, dark green spectra).

CONCLUSIONS

In conclusion, mild annealing of pristine and Ni or Fe dosed multilayers of squaric acid on Cu(100) to 393 K leads to Cu-, Ni- and Fe-squarate 2D MOFs. All three layers exist as two mirror domains with the same $(5 \mp 1; \pm 1\ 5)$ unit cells. Annealing leads to decomposition of the 2D MOFs into carbon monoxide. While copper squarate layers undergo regular decomposition, Ni- and Fe-squarate MOFs decompose autocatalytically resulting in very narrow TPRS peaks. Thereby, vacant sites adjacent to NiSq and FeSq catalyze the decomposition of the MOFs. The Fe MOF is more stable and has a 50 K higher decomposition temperature than the Ni MOF. Intriguingly, mixed {Fe+Ni}MOFs also decompose in one step and yield a single TPRS peak at an intermediate temperature. Insights into the autocatalytic interplay of vacancies and set-free metal atoms comes from "spatially-aware" kinetic modelling. Because more stable Fe-squarate blocks to some extent the vacancy-induced decomposition of Ni-squarate, the latter is stabilized until decomposition occurs simultaneously. To our knowledge, such interplay of vacancies plus protection by a more stable species is unprecedented in surface explosion.

With squarate as small ligand, the MOFs have relatively high metal densities (M−M distance 7.7 Å, M = {Fe, Ni}). Such aspect make these systems promising as catalysts for energy conversion chemistry.[50–52] For Fe and Ni MOFs, the small inter atomic distances cause strong magnetic interactions, making them interesting candidates for studies of 2D magnetism.[53,54]

ASSOCIATED CONTENT

Supporting Information

The following files are available free of charge.

Detailed experimental methods, detailed discussion on the M 2p binding energies, full description of the spatial and rate equation models (PDF)

Movies depicting the decomposition of {Ni, Ni+Fe, Fe}Sq layers simulated by the spatial model (MP4 files packed as ZIP)

AUTHOR INFORMATION

Corresponding Authors

Christian Wäckerlin

Surface Science and Coating Technologies, Empa, Swiss Federal Laboratories for Materials Science and Technology, Überlandstrasse 129, 8600 Dübendorf, Switzerland; orcid.org/0000-0001-6587-1235; E-mail: christian.waeckerlin@empa.ch

Karl-Heinz Ernst

Surface Science and Coating Technologies, Empa, Swiss Federal Laboratories for Materials Science and Technology, Überlandstrasse 129, 8600 Dübendorf, Switzerland; Department of Chemistry, University of Zurich, 8057 Zurich, Switzerland; Institute of Physics of the Czech Academy of Sciences, Cukrovarnická 10, 162 00 Praha 6, Czech Republic; orcid.org/0000-0002-2077-4922; E-mail: karl-heinz.ernst@empa.ch

Notes

The authors declare no competing financial interest.

ACKNOWLEDGMENTS

Financial support by the University Research Priority Program LightChEC of the University of Zürich, Switzerland, and the Swiss National Science Foundation (R'Equip, Sinergia) is gratefully acknowledged.

REFERENCES

(1) Yaghi, O. M.; O'Keeffe, M.; Ockwig, N. W.; Chae, H. K.; Eddaoudi, M.; Kim, J. Reticular Synthesis and the Design of New Materials. *Nature* **2003**, *423*, 705–714.

(2) Fujita, M.; Umemoto, K.; Yoshizawa, M.; Fujita, N.; Kusukawa, T.; Biradha, K. Molecular Paneling via Coordination. *Chem. Commun.* **2001**, *6,* 509–518.

(3) Shekhah, O.; Liu, J.; Fischer, R. A.; Wöll, Ch. MOF Thin Films: Existing and Future Applications. *Chem. Soc. Rev.* **2011**, *40*, 1081–1106.

(4) Zacher, D.; Shekhah, O.; Wöll, C.; Fischer, R. A. Thin Films of Metal–Organic Frameworks. *Chem. Soc. Rev.* **2009**, *38*, 1418–1429.

(5) Gottfried, J. M. Surface Chemistry of Porphyrins and Phthalocyanines. *Surf. Sci. Rep.* **2015**, *70*, 259–379.

(6) Lang, R.; Li, T.; Matsumura, D.; Miao, S.; Ren, Y.; Cui, Y.-T.; Tan, Y.; Qiao, B.; Li, L.; Wang, A., et al. Hydroformylation of Olefins by a Rhodium Single-Atom Catalyst with Activity Comparable to $RhCl(PPh_3)_3$. *Angew Chem Int Ed* **2016**, *55*, 16054–16058.

(7) Cui, X.; Li, W.; Ryabchuk, P.; Junge, K.; Beller, M. Bridging Homogeneous and Heterogeneous Catalysis by Heterogeneous Single-Metal-Site Catalysts. *Nat. Catal.* **2018**, *1*, 385–397.

(8) West, R.; Niu, H.-Y.; Powell, D. L.; Evans, M. V. Symmetrical Resonance Stabilized Anions, $C_n O_n^{-2}$. *J. Am. Chem. Soc.* **1960**, *82*, 6204–6205.

(9) Seitz, G.; Imming, P. Oxocarbons and Pseudooxocarbons. *Chem. Rev.* **1992**, *92*, 1227–1260.

(10) West, R. Chemistry of the Oxocarbons. *Isr. J. Chem.* **1980**, *20*, 300–307.

(11) West, R. History of the Oxocarbons. In *Oxocarbons*; Academic Press, New York, 1980; pp 1–14.

(12) Schmidt, A. H. Oxokohlenstoffe. *Chem. Unserer Zeit* **1982**, *16*, 57–67.

(13) Junqueira, G. M. A.; Rocha, W. R.; De Almeida, W. B.; Dos Santos, H. F. Theoretical Analysis of the Oxocarbons: The Solvent and Counter-Ion Effects on the Structure and Spectroscopic Properties of the Squarate Ion. *Phys. Chem. Chem. Phys.* **2003**, *5*, 437–445.

(14) Skujins, S.; Webb, G. A. The Electronic Structures of Some Monocyclic Oxocarbons. *Spectrochim Acta* **1968**, *25A*, 917–924.

(15) Butlerow, A. Formation Synthétique d'une Substance Sucrée. *Comptes Rendus Chim.* **1861**, *53*, 145–147.

(16) Butlerow, A. Bildung einer zuckerartigen Substanz durch Synthese. *Ann. Chem. Pharm.* **1861**, *120*, 295–298.

(17) Soai, K.; Kawasaki, T.; Matsumoto, A. Asymmetric Autocatalysis of Pyrimidyl Alkanol and Its Application to the Study on the Origin of Homochirality. *Acc. Chem. Res.* **2014**, *47*, 3643–3654.

(18) McCarty, J.; Falconer, J.; Madix, R. J. Decomposition of Formic Acid on Ni(110) I. Flash Decomposition from the Clean Surface and Flash Desorption of Reaction Products. *J. Catal.* **1973**, *30*, 235–249.

(19) Falconer, J.; McCarty, J.; Madix, R. J. The Explosive Decomposition of Formic Acid on Clean Ni(110). *Jpn. J. Appl. Phys.* **1974**, *13*, 525/1-4.

(20) Aas, N.; Bowker, M. Adsorption and Autocatalytic Decomposition of Acetic Acid on Pd(110). *J. Chem. Soc. Faraday Trans.* **1993**, *89*, 1249–1255.

(21) Li, Y.; Bowker, M. Acetic Acid on Rh(110): The Stabilization and Autocatalytic Decomposition of Acetate. *J. Catal.* **1993**, *142*, 630–640.

(22) Madix, R. J.; Falconer, J. L.; Suszko, A. M. The Autocatalytic Decomposition of Acetic Acid on Ni(110). *Surf. Sci.* **1976**, *54*, 6–20.

(23) Gellman, A. J.; Ernst, K.-H. Chiral Autocatalysis and Mirror Symmetry Breaking. *Catal Lett* **2018**, *148*, 1610–1621.

(24) Bowker, M.; Morgan, C.; Couves, J. Acetic Acid Adsorption and Decomposition on Pd(110). *Surf. Sci.* **2004**, *555*, 145–156.

(25) Yun, Y.; Gellman, A. J. Adsorption-Induced Auto-Amplification of Enantiomeric Excess on an Achiral Surface. *Nat. Chem.* **2015**, *7*, 520–525.

(26) Bowker, M.; Madix, R. XPS, UPS and Thermal Desorption Studies of the Adsorption and Reactions of CH_3CHO and CH_3COOH with the Cu(110) Surface. *Vacuum* **1981**, *31*, 711–714.

(27) Youngs, T. G. A.; Haq, S.; Bowker, M. Formic Acid Adsorption and Oxidation on Cu(110). *Surf. Sci.* **2008**, *602*, 1775–1782.

(28) Lesley, M. W.; Schmidt, L. D. The NO + CO Reaction on Pt(100). *Surf. Sci.* **1985**, *155*, 215–240.

(29) M.W. Lesley; L.D. Schmidt. Chemical Autocatalysis in the NO + CO Reaction on Pt(100). *Chem. Phys. Lett.* **1983**, *102*, 459–463.

(30) Mairena, A.; Wienke, M.; Martin, K.; Avarvari, N.; Terfort, A.; Ernst, K.-H.; Wäckerlin, C. Stereospecific Autocatalytic Surface Explosion Chemistry of Polycyclic Aromatic Hydrocarbons. *J. Am. Chem. Soc.* **2018**, *140*, 7705–7709.

(31) Cohen, S.; Lacher, J. R.; Park, J. D. Diketocyclobutenediol. *J. Am. Chem. Soc.* **1959**, *81*, 3480–3480.

(32) Stepanow, S.; Strunskus, T.; Lingenfelder, M.; Dmitriev, A.; Spillmann, H.; Lin, N.; Barth, J. V.; Wöll, Ch.; Kern, K. Deprotonation-Driven Phase Transformations in Terephthalic Acid Self-Assembly on Cu(100). *J. Phys. Chem. B* **2004**, *108*, 19392–19397.

(33) Rieger, A.; Sax, C.; Bauert, T.; Wäckerlin, C.; Ernst, K.-H. Chiral Molecules Adsorbed on a Solid Surface: Tartaric Acid Diastereomers and Their Surface Explosion on Cu(111). *Chirality* **2018**, *30*, 369–377.

(34) Rieger, A.; Schnidrig, S.; Probst, B.; Ernst, K.-H.; Wäckerlin, C. Ranking the Stability of Transition Metal Complexes by On-Surface Atom Exchange. *J. Phys. Chem. Lett.* **2017**, *8*, 6193–6198.

(35) Li, J.; Wäckerlin, C.; Schnidrig, S.; Joliat, E.; Alberto, R.; Ernst, K.-H. On-Surface Metalation and 2D Self-Assembly of Pyrphyrin Molecules Into Metal-Coordinated Networks on Cu(111). *Helv. Chim. Acta* **2017**, *100*, e1600278/1-8.

(36) Diller, K.; Klappenberger, F.; Marschall, M.; Hermann, K.; Nefedov, A.; Wöll, Ch.; Barth, J. V. Self-Metalation of 2H-Tetraphenylporphyrin on Cu(111): An x-Ray Spectroscopy Study. *J. Chem. Phys.* **2012**, *136*, 014705/1-13.

(37) Lin, N.; Dmitriev, A.; Weckesser, J.; Barth, J. V.; Kern, K. Real-Time Single-Molecule Imaging of the Formation and Dynamics of Coordination Compounds. *Angew. Chem. Int. Ed.* **2002**, *41*, 4779–4783.

(38) Tait, S. L.; Wang, Y.; Costantini, G.; Lin, N.; Baraldi, A.; Esch, F.; Petaccia, L.; Lizzit, S.; Kern, K. Metal−Organic Coordination Interactions in Fe−Terephthalic Acid Networks on Cu(100). *J. Am. Chem. Soc.* **2008**, *130*, 2108–2113.

(39) Shchyrba, A.; Wäckerlin, C.; Nowakowski, J.; Nowakowska, S.; Björk, J.; Fatayer, S.; Girovsky, J.; Nijs, T.; Martens, S. C.; Kleibert, A., et al. Controlling the Dimensionality of On-Surface Coordination Polymers via Endo- or Exoligation. *J. Am. Chem. Soc.* **2014**, *136*, 9355–9363.

(40) Santhini, V. M.; Wäckerlin, C.; Cahlík, A.; Ondráček, M.; Pascal, S.; Matěj, A.; Stetsovych, O.; Mutombo, P.; Lazar, P.; Siri, O., et al. 1D Coordination π-d Conjugated Polymers with Distinct Structures Defined by the Choice of the Transition Metal: Towards a New Class of Antiaromatic Macrocycles. *Angew. Chem. Int. Ed.* **2020**, *60*, 439–445.

(41) West, Robert.; Niu, H. Ying. New Aromatic Anions. VII. Complexes of Squarate Ion with Some Divalent and Trivalent Metals. *J. Am. Chem. Soc.* **1963**, *85*, 2589–2590.

(42) Moulder, J. *Handbook of X-Ray Photoelectron Spectroscopy: A Reference Book of Standard Spectra for Identification and Interpretation of XPS Data*; Physical Electronics Division Perkin-Elmer Corp.: Eden Prairie Minn., 1992.

(43) Grosvenor, A. P.; Kobe, B. A.; Biesinger, M. C.; McIntyre, N. S. Investigation of Multiplet Splitting of Fe 2p XPS Spectra and Bonding in Iron Compounds. *Surf. Interface Anal.* **2004**, *36*, 1564–1574.

(44) Merz, L.; Ernst, K.-H. Unification of the Matrix Notation in Molecular Surface Science. *Surf. Sci.* **2010**, *604*, 1049–1054.

(45) Jensen, F.; Besenbacher, F.; Laegsgaard, E.; Stensgaard, I. Dynamics of Oxygen-Induced Reconstruction of Cu(100) Studied by Scanning Tunneling Microscopy. *Phys. Rev. B* **1990**, *42*, 9206–9209.

(46) Tero, R.; Sasaki, T.; Iwasawa, Y. CO Adsorption on c(2×2)-Li/Cu(100): Interaction between CO and Li on Unreconstructed Cu(100) Surfaces. *Surf. Sci.* **2000**, *448*, 250–260.

(47) Mhatre, B. S.; Pushkarev, V.; Holsclaw, B.; Lawton, T. J.; Sykes, E. C. H.; Gellman, A. J. A Window on Surface Explosions: Tartaric Acid on Cu(110). *J. Phys. Chem. C* **2013**, *117*, 7577–7588.

(48) Sharpe, R. G.; Bowker, M. Kinetic Models of Surface Explosions. *J. Phys. Condens. Matter* **1995**, *7*, 6379–6392.

(49) King, D. A. Thermal Desorption from Metal Surfaces: A Review. *Surf. Sci.* **1975**, *47*, 384–402.

(50) Gutzler, R.; Stepanow, S.; Grumelli, D.; Lingenfelder, M.; Kern, K. Mimicking Enzymatic Active Sites on Surfaces for Energy Conversion Chemistry. *Acc. Chem. Res.* **2015**, *48*, 2132–2139.

(51) Wurster, B.; Grumelli, D.; Hötger, D.; Gutzler, R.; Kern, K. Driving the Oxygen Evolution Reaction by Nonlinear Cooperativity in Bimetallic Coordination Catalysts. *J. Am. Chem. Soc.* **2016**, *138*, 3623–3626.

(52) Hötger, D.; Etzkorn, M.; Morchutt, C.; Wurster, B.; Dreiser, J.; Stepanow, S.; Grumelli, D.; Gutzler, R.; Kern, K. Stability of Metallo-Porphyrin Networks under Oxygen Reduction and Evolution Conditions in Alkaline Media. *Phys. Chem. Chem. Phys.* **2019**, *21*, 2587–2594.

(53) Abdurakhmanova, N.; Tseng, T.-C.; Langner, A.; Kley, C. S.; Sessi, V.; Stepanow, S.; Kern, K. Superexchange-Mediated Ferromagnetic Coupling in Two-Dimensional Ni-TCNQ Networks on Metal Surfaces. *Phys. Rev. Lett.* **2013**, *110*, 027202/1-5.

(54) Umbach, T. R.; Bernien, M.; Hermanns, C. F.; Krüger, A.; Sessi, V.; Fernandez-Torrente, I.; Stoll, P.; Pascual, J. I.; Franke, K. J.; Kuch, W. Ferromagnetic Coupling of Mononuclear Fe Centers in a Self-Assembled Metal-Organic Network on Au(111). *Phys. Rev. Lett.* **2012**, *109*, 267207/1-5.